ACS APPLIED MATERIALS & INTERFACES

Research Article

Cite This: ACS Appl. Mater. Interfaces 2018, 10, 20783−20789

www.acsami.org

Opal-like Multicolor Appearance of Self-Assembled Photonic Array

Zohar A. Arnon,[†] Dorothea Pinotsi,[‡,◆] Matthias Schmidt,[§] Sharon Gilead,[†] Tom Guterman,[†] Aditya Sadhanala,[⊥] Shahab Ahmad,[#,▲] Aviad Levin,[†] Paul Walther,[∥] Clemens F. Kaminski,[‡] Marcus Fändrich,[§] Gabriele S. Kaminski Schierle,[‡] Lihi Adler-Abramovich,[○] Linda J. W. Shimon,[¶] and Ehud Gazit*[,†,▽]

[†]Department of Molecular Microbiology and Biotechnology, George S. Wise Faculty of Life Sciences, Tel Aviv University, Tel Aviv 6997801, Israel

[‡]Department of Chemical Engineering and Biotechnology, University of Cambridge, Cambridge CB3 0AS, United Kingdom

[§]Institute of Protein Biochemistry, Ulm University, Ulm 89081, Germany

[⊥]Cavendish Laboratory, Department of Physics, University of Cambridge, Cambridge CB3 0HE, United Kingdom

[#]Institute for Manufacturing, Department of Engineering, University of Cambridge, Cambridge CB3 0FS, United Kingdom

[∥]Central Facility for Electron Microscopy, Ulm University, Ulm 89081, Germany

[○]Department of Oral Biology, The Goldschleger School of Dental Medicine, Sackler Faculty of Medicine, Tel Aviv University, Tel Aviv 6997801, Israel

[¶]Department of Chemical Research Support, Weizmann Institute of Science, Rehovot 7610001, Israel

[▽]Department of Materials Science and Engineering, Iby and Aladar Fleischman Faculty of Engineering, Tel Aviv University, Tel Aviv 6997801, Israel

Supporting Information

ABSTRACT: Molecular self-assembly of short peptide building blocks leads to the formation of various material architectures that may possess unique physical properties. Recent studies had confirmed the key role of biaromaticity in peptide self-assembly, with the diphenylalanine (FF) structural family as an archetypal model. Another significant direction in the molecular engineering of peptide building blocks is the use of fluorenylmethoxycarbonyl (Fmoc) modification, which promotes the assembly process and may result in nanostructures with distinctive features and macroscopic hydrogel with supramolecular features and nanoscale order. Here, we explored the self-assembly of the protected, noncoded fluorenylmethoxycarbonyl-β,β-diphenyl-Ala-OH (Fmoc-Dip) amino acid. This process results in the formation of elongated needle-like crystals with notable aromatic continuity. By altering the assembly conditions, arrays of spherical particles were formed that exhibit strong light scattering. These arrays display vivid coloration, strongly resembling the appearance of opal gemstones. However, unlike the Rayleigh scattering effect produced by the arrangement of opal, the described optical phenomenon is attributed to Mie scattering. Moreover, by controlling the solution evaporation rate, i.e., the assembly kinetics, we were able to manipulate the resulting coloration. This work demonstrates a bottom-up approach, utilizing self-assembly of a protected amino acid minimal building block, to create arrays of organic, light-scattering colorful surfaces.

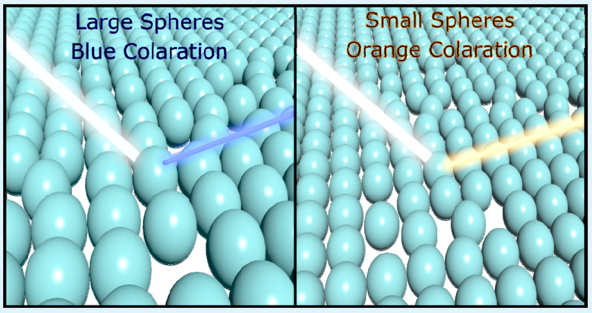

KEYWORDS: *self-assembly, Mie scattering, colored surfaces, microspheres, biaromatic amino acid, amino acid self-assembly, Fmoc modification, opal-like*

1. INTRODUCTION

Recent advances in bioorganic nanotechnology have established the notion that very simple building blocks, such as dipeptides, can form regular nanostructures with distinct mechanical, optical, piezoelectric, and electronic properties.[1−3] In particular, members of the diphenylalanine (FF) dipeptide archetypal family have been shown to form various morphologies and ordered nanostructures such as tubes, rods, fibrils, spheres, plates, and macroscopic hydrogels with nanoscale order.[4−8] Recent studies have demonstrated the control over rod-like assemblies, as well as the rational prediction of toroid-like assemblies.[9−11] Some of these structures exhibit remarkable physicochemical features, including high thermal stability,

Received: March 26, 2018
Accepted: May 29, 2018
Published: May 29, 2018

Downloaded via UNIV OF CAMBRIDGE on September 18, 2019 at 09:41:03 (UTC).
See https://pubs.acs.org/sharingguidelines for options on how to legitimately share published articles.

© 2018 American Chemical Society

DOI: 10.1021/acsami.8b04912
ACS Appl. Mater. Interfaces 2018, 10, 20783−20789

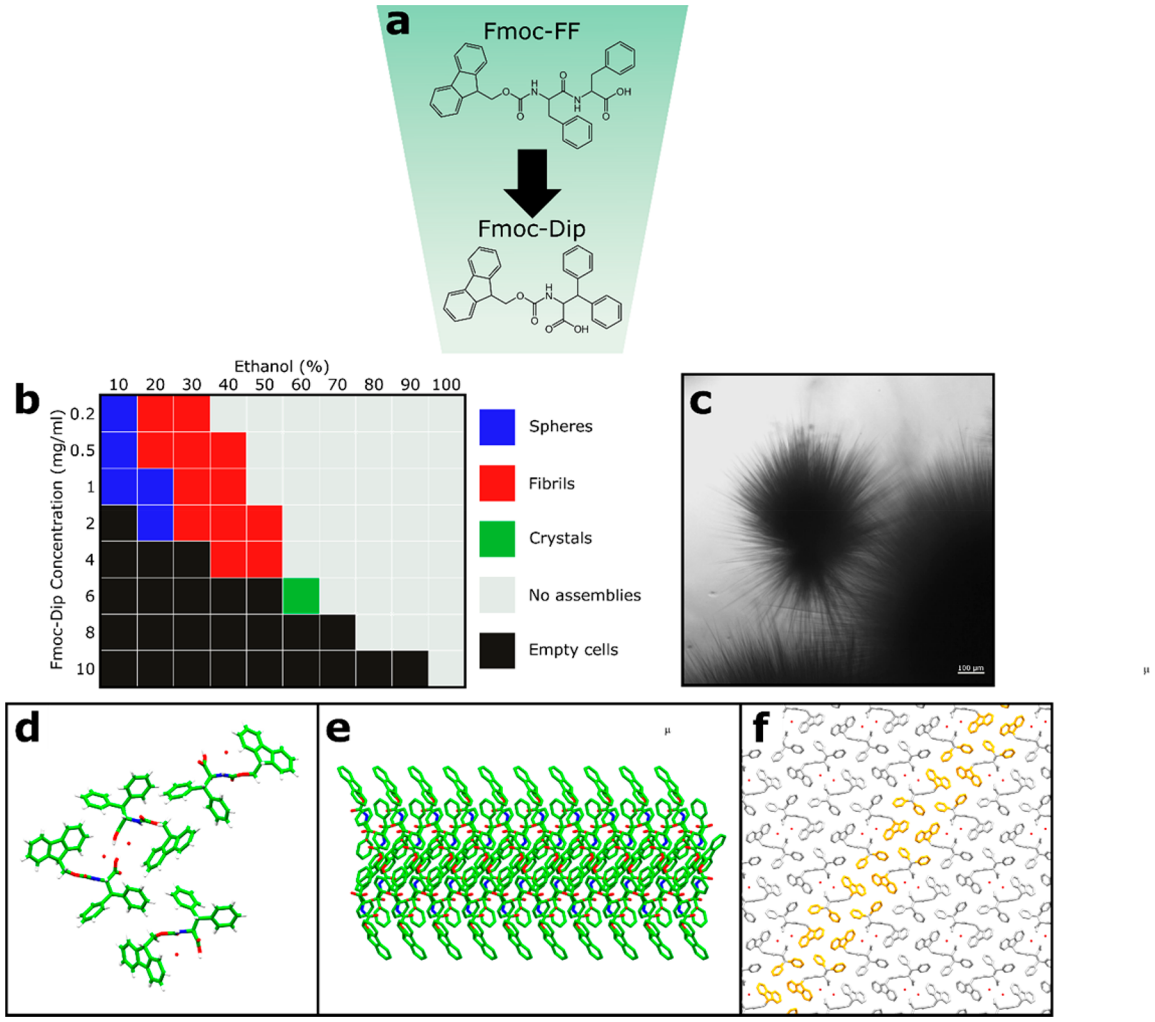

Figure 1. Structure of Fmoc-Dip needle-like crystals. (a) Fmoc-FF and Fmoc-Dip molecular scheme. (b) Phase diagram of 55 assembly conditions and the corresponding structures in solution taken 72 h following sample preparation. Assembly conditions determine the kinetics and morphology: spheres (blue), fibrils (red), and needle-like crystal aggregates (green). The white area represents conditions in which no assemblies were visible. In black are conditions that could not be achieved with the initial stock solution of 10 mg/mL Fmoc-Dip in EtOH. (c) Needle-like crystals propagating from a nucleation site. Scale bar is 100 μm. (d–f) Crystal structure of Fmoc-Dip determined using X-ray scattering. View of the unit cell as determined for single Fmoc-Dip needle-like crystals (d). Crystal packing down the crystallographic *c* axis (e). Aromatic rings (orange) to display the aromatic continuity within the crystal, as viewed down the *a* axis (f).

metallic-like mechanical rigidity, luminescence, piezoelectricity, and semiconductivity.[12−17]

The importance of aromatic moieties in facilitating and modulating self-assembly has been previously demonstrated, both theoretically as well as experimentally.[11,18] In a comprehensive study, a nonbiased exploration of all 8 000 tripeptide combinations composed of the 20 coded amino acids revealed the contribution of aromatic pairs in promoting self-assembly into ordered structures.[19] Importantly, all 10 top-scored tripeptides contain a pair of aromatic residues; in all cases, phenylalanine paired with another phenylalanine, tryptophan, or tyrosine.

In addition to the amino acid nature, terminal cap aromaticity was also found to significantly modulate the self-assembly of bioorganic building blocks.[10,20−22] N-terminal capping with an Fmoc moiety is one of the most studied modifications that affect peptide self-assembly.[23] Modification of very short peptides, and even single amino acids, with this moiety promotes their efficient assembly into ordered nanometric architectures, possessing distinctive physical properties.[24]

Recently, there has been an increased interest in bioorganic self-assembly systems that exhibit optical features, such as photoluminescence[15,16,25,26] and waveguidance.[3] FF assemblies can act as an active optical waveguiding material, allowing locally excited states to propagate along the axis of the assemblies.[3] In addition, Fmoc-capped building blocks were shown to display remarkable optical properties, such as quantum confinement and fluorescence.[27]

The ability of FF to self-assemble into ordered structures was discovered by a systematic reductionist exploration of biological recognition modules in an amyloidogenic polypeptide.[28] Applying a similar reductionist approach, we explore here the possibility of substituting the aromatic pair of self-assembling dipeptides with a biaromatic side chain of a single amino acid. This is in line with the recent interest in amino acid materials that show remarkable physical properties.[29−31]

DOI: 10.1021/acsami.8b04912
ACS Appl. Mater. Interfaces 2018, 10, 20783−20789

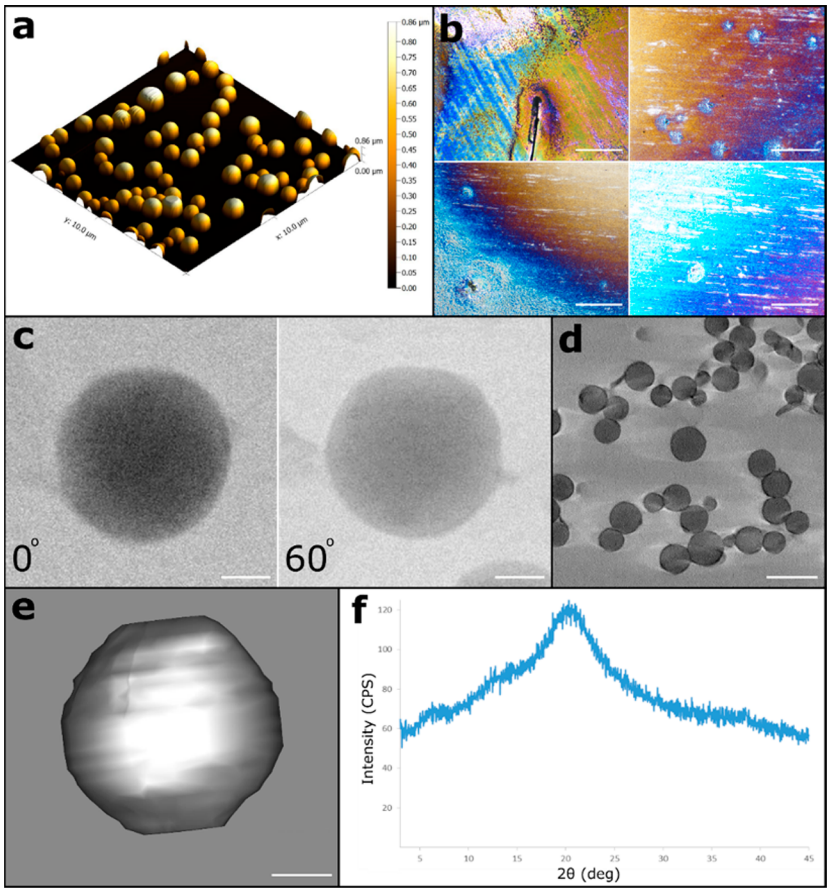

Figure 2. Fmoc-Dip spheres. (a) AFM micrograph of an array of spheres. (b) Bright-field microscopy image of the sphere array at low magnification (×4). Scale bars are 500 μm. (c) STEM image of a single sphere at 0° and 60° tilt. Scale bars are 100 nm. (d) Virtual cross section of the STEM tomogram. Scale bar is 500 nm. (e) 3D image constructed from a tilt image sequence (−72° to 72°, increment 1.5°). (f) Powder XRD spectrum exhibiting a characteristic amorphous peak.

2. EXPERIMENTAL SECTION

2.1. Fmoc-Dip Crystallization. Fluorenylmethoxycarbonyl-β,β-diphenyl-Ala-OH (Fmoc-Dip, Bachem) stock solutions were prepared in absolute ethanol, diluted into double-distilled water at a 1:1 ratio, and incubated in a polypropylene conical tube at room temperature for several weeks. The resulting colorless, needle-like crystals were visible on the tube−solution interface. The structural morphology was determined using bright-field microscopy.

2.2. Single-Crystal X-ray Diffraction. The Fmoc-Dip crystal was transferred to Paratone oil (Hampton Research), mounted on a MiTeGen loop, and flash frozen in liquid nitrogen. Crystal data for Fmoc-Dip measured at 100 K on a Bruker D8 Venture diffractometer equipped with [λ (CuKα) = 0.154184 Å] radiation. The data were processed with Bruker D8 Venture suite. The structure was solved by direct methods with SHELXT-2013 and refined with full-matrix least-squares refinement based on F2 with SHELXL-2013. Crystallographic data are presented in Table S1 and are available from the CCDC with deposition numbers 1557856.

2.3. Atomic Force Microscopy. Topography measurements by atomic force microscopy (AFM) were performed using a JPK research AFM (model NanoWizard III) in the force spectroscopy mode. Gwyddion software version 2.37 was used to create the AFM images.

2.4. Scanning Transmission Electron Microscopy Tomography. A solution of 10 mg/mL of Fmoc-Dip in 100% EtOH was prepared. A sample 20 μL of the solution was dried on a glass slide to form spheres. The spheres were scraped off, taken up in 50% EtOH, and dried on a 3 mm transmission electron microscopy (TEM) copper grid with a hole of 1 mm diameter covered with a layer of carbon on top of a Formvar film. The tilt-series was collected on a JEM-2100F electron microscope (JEOL) operated at an acceleration voltage of 200 kV in the scanning transmission mode. Electron micrographs were recorded with a bright-field detector at a pixel size of 2.74 nm. A tilt-series was recorded from −72° to +72° at increments of 1.5°. The tomogram was created out of 96 images using the IMOD software package.[32] Images were first aligned to an image stack and then computationally reconstructed using a weighted back-projection algorithm to form the tomogram.

2.5. X-ray Powder Diffraction. A sample of Fmoc-Dip 10 mg/mL in 100% EtOH was dried on a Si zero-background holder (Si single-crystal wafer, which surface is (510) plane). Diffraction measurements were carried out in reflection geometry using a TTRAX III (Rigaku, Japan) diffractometer equipped with a rotating Cu anode, operating at 50 kV/200 mA. A bent graphite monochromator and scintillation detector were aligned in the diffracted beam. $\theta/2\theta$ scans were performed under specular conditions in the Bragg brentano mode with variable slits. The 2θ scanning range was 3−45° with step size 0.025° and collection time of 15 s per step.

2.6. High-Resolution Scanning Electron Microscopy. Samples of tetra-F and penta-F solutions at 1:25 and 1:5 AcOH/water ratios, respectively, were placed on glass slides and were left to dry at room temperature. Samples were then coated with Cr and viewed using a JSM-6700 field-emission high-resolution scanning electron microscope (HR-SEM) (Jeol, Tokyo, Japan), equipped with a cold field emission gun, operating at 10 kV.

2.7. Image Analysis. HR-SEM images were analyzed using ImageJ 1.45S. Sphere diameter distribution was measured using *Analyze Particles* function of the software, and edges were excluded. Filters of circularity (0.2−1) and particle size (0.1−∞ μm) were applied.

2.8. Confocal Microscopy and Spectral Imaging. Spatially resolved images of the intrinsic fluorescence of spheres dried on a glass

DOI: 10.1021/acsami.8b04912
ACS Appl. Mater. Interfaces 2018, 10, 20783−20789

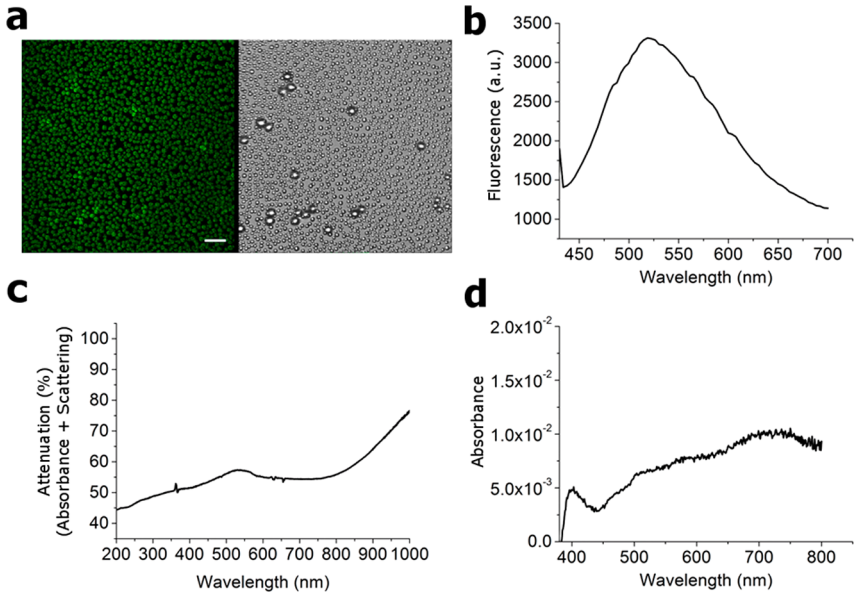

Figure 3. (a) Fluorescence (left) and differential interference contrast (DIC) (right) images of the sphere array. Scale bar is 10 μm. (b) Corresponding emission spectrum. Excitation at 405 nm. (c) Standard total attenuation spectrum of Fmoc−Dip sphere array, taken using a UV−vis spectrophotometer. The probe wavelength was scanned in the range of 200−1000 nm, and the total transmission was measured. (d) Absorption spectrum of a Fmoc-Dip sphere array film, deposited on a quartz coverslip, measured by using an integrating sphere equipped spectrophotometer. The wavelength was scanned in the range of 400−800 nm.

slide from a stock solution of 10 mg/mL Fmoc-Dip in EtOH were obtained using a confocal microscope (Leica TCS SP5, Leica Microsystems GmbH, Wetzlar, Germany), with a 405 nm diode laser as the excitation source and a 63×, 1.4 NA oil immersion objective. For the spectral measurements, an emission bandwidth of 20 nm was used in the range of 430−600 nm.

2.9. Optical Measurements. The UV−vis absorption measurements were performed using a Hewlett−Packard HP845x vis−UV spectrometer in the range of 500−570 nm. The integrating sphere absorption measurements were performed using a commercial PerkinElmer lambda 750 UV−vis−NIR setup equipped with a light source (tungsten−halogen and deuterium), a conventional photomultiplier (PMT) detector, a 10 cm integrating sphere module attachment, a monochromator, and a detector slit width of 10 nm. All measurements were performed under standard ambient conditions. Films were prepared by drop-casting the samples, dissolved in the appropriate solvents, on the quartz/glass slide substrate. The transmitted light was corrected using a reference of an empty quartz coverslip of the same type and thickness as the substrate used for the sample.

2.10. Optical Microscopy. Images were taken using a Nikon Eclipse Ti-E inverted microscope. Large image was stitched at 10% overlap of 24 × 31 individual ×4 images. The controlled evaporation rate was maintained using a controlled air pump and a H301-K-Frame chamber from Okolab.

3. RESULTS AND DISCUSSION

As a minimal model, we studied the self-assembly of the protected noncoded Fmoc-Dip amino acid (Figure 1a). Fmoc-Dip was found to have very limited solubility in pure water yet exhibits high solubility in ethanol (EtOH). This property was utilized for triggering the self-assembly of the amino acid using a solvent-switch method, whereby a concentrated Fmoc-Dip in EtOH stock solution was diluted into water and the assembly was monitored. Altering the self-organization conditions by varying the EtOH/water ratio or the concentration of Fmoc-Dip building block, dramatically affected the morphology of the formed assemblies. Fmoc-Dip can form spheres, as well as entangled fibrils or needle-like crystals, depending on the exact solution conditions (Figures 1b and c and S1). This typical phase diagram is consistent with the organization of the building blocks into supramolecular polymers and phase organization as observed in model peptide systems.[6,33,34]

Single-crystal X-ray diffraction (XRD) analysis of an individual needle-like crystal revealed remarkable aromatic continuity throughout the crystal packing (Figure 1d−f). In addition, water molecules were incorporated in the unit cell, forming a network of hydrogen bonds with the Fmoc-Dip molecules. A central role for aromatic interactions and hydrogen bonds is clearly demonstrated, similar to FF crystal structure determined by Görbitz.[35] It was suggested that, under aqueous conditions, a three-dimensional aromatic stacking arrangement is achieved through interactions between planar and rigid phenyl rings within the FF crystal. This arrangement serves as a molecular adhesive (referred to as "aromatic glue") between the cylinder's hydrogen-bonded main chains, significantly stabilizing the structures.

Of the distinct morphological entities Fmoc-Dip formed under different solution conditions, we observed the organization of an array of spherical assemblies upon drying of 10 mg/mL of Fmoc-Dip in pure EtOH. Atomic force microscopy (AFM) analysis demonstrated that the spheres vary in size, ranging from a few hundred nanometers to 2 μm in diameter (Figure 2a). Interestingly, similarly sized spheres are mostly found in close proximity to each other, resulting in areas showing narrow sphere diameter distribution. Examination of the formed array using optical microscopy revealed a vivid set of colors at different areas of the sample. The colors were mainly blue and orange, but also green, red, and purple areas could be observed (Figure 2b). At higher magnifications, no colors were visible, indicating that this opal-like coloration is generated by the additive effect of several spheres within the array and not due to an intrinsic property of a single sphere. The virtual section of a tomogram and the constructed 3D image obtained from a series of images recorded by scanning

DOI: 10.1021/acsami.8b04912
ACS Appl. Mater. Interfaces 2018, 10, 20783−20789

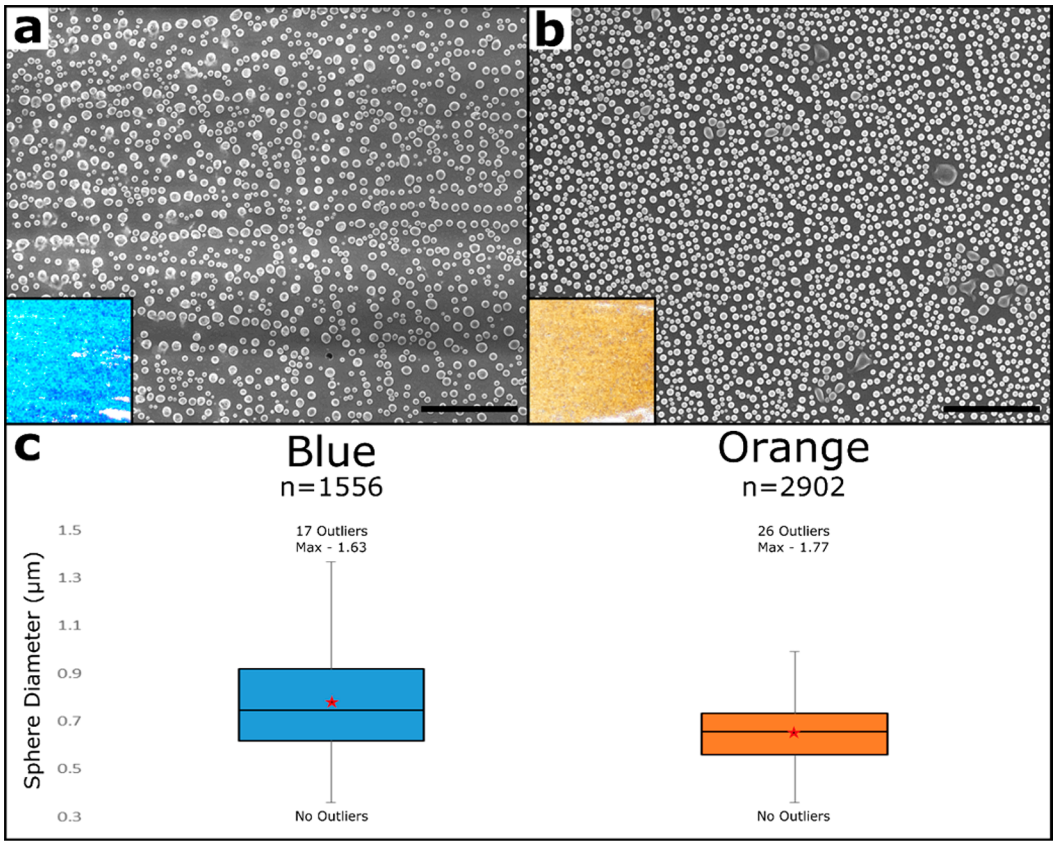

Figure 4. Correlation between sphere diameter and observed coloration. (a,b) Representative SEM micrographs of arrays exhibiting blue (a) and orange coloration (b). Scale bars represent 10 μm. (c) Box plot displays of sphere diameter size distribution obtained by image analysis. The mean value is annotated by a red star.

transmission electron microscopy (STEM) at different tilt angles (Figure 2c–e and Videos S1 and S2) shows that the particles are nearly perfect spheres and homogeneously solid. In addition, powder XRD of an array of spheres reveals that the spheres are amorphous and have no crystalline organization (Figure 2f).

Next, we examined the fluorescent properties of the individual spheres in further detail. For that purpose, we deposited samples of a stock solution containing 10 mg/mL of Fmoc-Dip in EtOH in small wells and allowed for their evaporation. A confocal microscope coupled with spectrometer was used to obtain the fluorescence spectra of these structures (Figure 3a). On the basis of previously shown excitation of similar fluorescent self-assembled protein structures,[15] the laser excitation wavelength was set to 405 nm and emission was scanned in the range of 430–600 nm with a 20 nm bandwidth. Several regions were clearly visible on the glass coverslip, featuring spheres of different sizes, as observed using AFM (Figure 2a). The emission spectra of all regions were similar, featuring a peak at 520 nm.

We then investigated the absorbance of the Fmoc-Dip sphere arrays employing two different methods of measurements. An absorbance spectrum using a conventional UV–vis spectrophotometer was first obtained (Figure 3c), showing an attenuation of the transmitted signal in the range of 500–570 nm. However, this method cannot distinguish between pure absorption and scattering that stems from the array itself. To obtain absorbance spectrum that excludes scattering, we also performed an absorbance measurement using an integrating sphere spectrophotometer (Figure 3d). In both experiments, the sphere arrays were produced as films, prepared by drop-casting the samples on a quartz coverslip substrate (see Experimental Section 2.9). According to the integrating sphere absorbance measurements, a very weak absorption peak could be observed at the range of ca. 400–420 nm, in agreement with the fluorescence measurements using laser excitation at 405 nm. The pronounced scattering at the range of 500–570 nm is in agreement with the colors observed with these sphere arrays.

We then aimed to investigate the structural differences between distinct colored areas. For this purpose, areas of the arrays exhibiting either blue or orange colors were studied in detail by scanning electron microscopy (Figure 4a and b). From the micrographs, it is clear that spheres at the blue areas are larger than those at the orange ones. Image analysis confirms that the mean diameter of spheres in the orange area is smaller, and with a narrower size distribution (0.65 $\pm$ 0.13 μm), than that of spheres in the blue area (0.77 $\pm$ 0.22 μm) (Figure 4c). In both cases, the diameter of the spheres is within the scale of visible light wavelengths. Taken together with the optical properties portrayed in Figure 3, this analysis indicates that the coloration of the sphere arrays results from Mie scattering, a phenomenon describing the scattering of electromagnetic radiation by particles of comparable size to the radiation wavelength.[36] According to the theory, light interacts with spherical particles and the scattered light, both transmitted and reflected, depends on the size of the scattering particles. This phenomenon was demonstrated in inorganic materials, such as wurtzite zinc oxide spheres of different sizes.[37−39] To validate the occurrence of Mie scattering by spherical particles at the scale of the scattered wavelength, arrays of commercially

DOI: 10.1021/acsami.8b04912
ACS Appl. Mater. Interfaces 2018, 10, 20783–20789

available monodispersed polystyrene (0.46 and 0.8 μm) and of silicon dioxide (0.5 and 1 μm) beads were similarly investigated. Bright-field microscopy images show that beads of diameters of 0.46 and 0.5 μm transmitted an orange color, while the 0.8 and 1 μm beads transmitted blue colors (Figure S2).

Because the particle size distribution at a certain area determines the observed color, we aimed to manipulate the distribution of sphere diameters by regulating the assembly conditions. The assembly conditions may be regulated by adjusting the temperature, humidity, molecular concentration, etc., in order to achieve a desired size. As a proof of concept, samples of Fmoc-Dip in EtOH were subjected to a constant air flow in order to induce EtOH evaporation. By altering the evaporation rate, a clear change in coloration was observed. When EtOH evaporation was promoted, arrays exhibiting orange coloration were prominent throughout the sample, while blue coloration was abundant in samples that were not subjected to active air flow (Figure S3). We assume that slower evaporation allows molecules to continue the diffusion in solution, thus organizing into larger spheres, resulting in blue coloration. On the other hand, relatively fast evaporation restricts the growth of the spheres, and thus orange coloration is observed with smaller diameter assemblies.

4. CONCLUSION

In conclusion, we describe here the self-association of Fmoc-Dip, a protected biaromatic single amino acid, into discrete structural entities, and their resulting properties were determined. Single-crystal XRD revealed the continuity of the aromatic interactions within the needle-like crystal structure. Altering the assembly conditions resulted in profoundly different assembly morphologies, including an array of spherical nanostructures, which displayed vivid opal-like coloration. We suggest that the observed colors stem from the scattering of polychromatic light, with dependency on particle size, whereby different sphere dimensions lead to the scattering of different wavelengths. The colors of the sphere array are sufficiently intense to be observed by the naked eye. To our knowledge, we investigate for the first time the self-assembly of a protected biaromatic single amino acid. This dynamic assembly process can be regulated with relative ease due to the simplicity of the described system. This spontaneous process may give rise to diverse morphological architectures and notable optical properties, with direct dependence on the assembly conditions. Moreover, the current system may offer a partial direction for coupling light emission into allowed Mie modes of a spherical resonator, which is superior to doping or other current techniques. Fmoc-Dip may be considered as a new member of the short self-assembling building block repertoire, as it further simplifies the assembling entity, while conserving the biaromatic moiety.

■ ASSOCIATED CONTENT

Supporting Information

The Supporting Information is available free of charge on the ACS Publications website at DOI: 10.1021/acsami.8b04912.

Crystallographic data and optical microscopy images (PDF)

Tilt-series tomogram from −72° to +72° at 1.5° increments of Fmoc-Dip spheres, using bright field (ZIP)

Tilt-series tomogram from −72° to +72° at 1.5° increments of Fmoc-Dip spheres, using dark field (ZIP)

CIF file for $C_{30}H_{25}NO_5$ (CIF)

■ AUTHOR INFORMATION

Corresponding Author

*E-mail: Ehudg@post.tau.ac.il.

ORCID

Zohar A. Arnon: 0000-0003-2915-5930

Aditya Sadhanala: 0000-0003-2832-4894

Gabriele S. Kaminski Schierle: 0000-0002-1843-2202

Lihi Adler-Abramovich: 0000-0003-3433-0625

Linda J. W. Shimon: 0000-0002-7861-9247

Present Addresses

◆D.P.: ScopeM Scientific Center for Optical and Electron Microscopy, ETH Zurich, Zurich CH8093, Switzerland.

▲S.A.: Centre for Nanoscience and Nanotechnology, Jamia Millia Islamia (A Central University), New Delhi, India 110025. E-mail: sahmad28@jmi.ac.in.

Notes

The authors declare no competing financial interest.

■ ACKNOWLEDGMENTS

This work was supported by the Israeli National Nanotechnology Initiative and Helmsley Charitable Trust (E.G.), the European Research Council BISON project (E.G.), and the Clore Scholarship program (Z.A.A.). This work is also supported by a grant from the Deutsche Forschungsgemeinschaft, SCHM 3276/1 (M.S.) This project has reveived funding from the European Union's Horizon 2020 research and innovation programme under Grant Agreement No. 722380 (C.F.K.). We would like to acknowledge EPSRC and Indo-UK APEX project for their support. The authors acknowledge technical assistance by Thomas Heerde, Ulm University, and Dr. Yishay Feldman, Weizmann Institute of Science. We thank Professor Sir Richard Friend and members of the Gazit and Adler-Abramovich groups for the helpful discussions.

■ REFERENCES

(1) Zhang, S. Fabrication of Novel Biomaterials through Molecular Self-Assembly. *Nat. Biotechnol.* **2003**, *21*, 1171−1178.

(2) Esin, A.; Baturin, I.; Nikitin, T.; Vasilev, S.; Salehli, F.; Shur, V. Y.; Kholkin, A. L. Pyroelectric Effect and Polarization Instability in Self-Assembled Diphenylalanine Microtubes. *Appl. Phys. Lett.* **2016**, *109*, 142902.

(3) Li, Q.; Jia, Y.; Dai, L.; Yang, Y.; Li, J. Controlled Rod Nanostructured Assembly of Diphenylalanine and Their Optical Waveguide Properties. *ACS Nano* **2015**, *9*, 2689−2695.

(4) Marchesan, S.; Vargiu, A. V.; Styan, K. E. The Phe-Phe Motif for Peptide Self-Assembly in Nanomedicine. *Molecules* **2015**, *20*, 19775−19788.

(5) Yan, X.; Zhu, P.; Li, J. Self-Assembly and Application of Diphenylalanine-Based Nanostructures. *Chem. Soc. Rev.* **2010**, *39*, 1877−1890.

(6) Levin, A.; Mason, T. O.; Adler-Abramovich, L.; Buell, A. K.; Meisl, G.; Galvagnion, C.; Bram, Y.; Stratford, S. A.; Dobson, C. M.; Knowles, T. P. J.; Gazit, E. Ostwald's Rule of Stages Governs Structural Transitions and Morphology of Dipeptide Supramolecular Polymers. *Nat. Commun.* **2014**, *5*, 5219.

(7) Reches, M.; Gazit, E. Self-Assembly of Peptide Nanotubes and Amyloid-like Structures by Charged-Termini-Capped Diphenylalanine Peptide Analogues. *Isr. J. Chem.* **2005**, *45*, 363−371.

DOI: 10.1021/acsami.8b04912
ACS Appl. Mater. Interfaces 2018, 10, 20783−20789

(8) Chen, C.; Liu, K.; Li, J.; Yan, X. Functional Architectures Based on Self-Assembly of Bio-Inspired Dipeptides: Structure Modulation and Its Photoelectronic Applications. *Adv. Colloid Interface Sci.* **2015**, *225*, 177−193.
(9) Arnon, Z. A.; Vitalis, A.; Levin, A.; Michaels, T. C. T.; Caflisch, A.; Knowles, T. P. J.; Adler-Abramovich, L.; Gazit, E. Dynamic Microfluidic Control of Supramolecular Peptide Self-Assembly. *Nat. Commun.* **2016**, *7*, 13190.
(10) Adler-Abramovich, L.; Marco, P.; Arnon, Z. A.; Creasey, R. C. G.; Michaels, T. C. T.; Levin, A.; Scurr, D. J.; Roberts, C. J.; Knowles, T. P. J.; Tendler, S. J. B.; Gazit, E. Controlling the Physical Dimensions of Peptide Nanotubes by Supramolecular Polymer Coassembly. *ACS Nano* **2016**, *10*, 7436−7442.
(11) Guo, C.; Arnon, Z. A.; Qi, R.; Zhang, Q.; Adler-Abramovich, L.; Gazit, E.; Wei, G. Expanding the Nanoarchitectural Diversity through Aromatic Di- and Tri-Peptide Coassembly: Nanostructures and Molecular Mechanisms. *ACS Nano* **2016**, *10*, 8316−8324.
(12) Hauser, C. A. E.; Zhang, S. Nanotechnology: Peptides as Biological Semiconductors. *Nature* **2010**, *468*, 516−517.
(13) Lee, J. S.; Yoon, I.; Kim, J.; Ihee, H.; Kim, B.; Park, C. B. Self-Assembly of Semiconducting Photoluminescent Peptide Nanowires in the Vapor Phase. *Angew. Chem., Int. Ed.* **2011**, *50*, 1164−1167.
(14) Nguyen, V.; Zhu, R.; Jenkins, K.; Yang, R. Self-Assembly of Diphenylalanine Peptide with Controlled Polarization for Power Generation. *Nat. Commun.* **2016**, *7*, 13566.
(15) Pinotsi, D.; Buell, A. K.; Dobson, C. M.; Kaminski Schierle, G. S.; Kaminski, C. F. A Label-Free, Quantitative Assay of Amyloid Fibril Growth Based on Intrinsic Fluorescence. *ChemBioChem* **2013**, *14*, 846−850.
(16) Pinotsi, D.; Grisanti, L.; Mahou, P.; Gebauer, R.; Kaminski, C. F.; Hassanali, A.; Kaminski Schierle, G. S. Proton Transfer and Structure-Specific Fluorescence in Hydrogen Bond-Rich Protein Structures. *J. Am. Chem. Soc.* **2016**, *138*, 3046−3057.
(17) Tao, K.; Makam, P.; Aizen, R.; Gazit, E. Self-Assembling Peptide Semiconductors. *Science (Washington, DC, U. S.)* **2017**, *358*, 885−893.
(18) Fleming, S.; Ulijn, R. V. Design of Nanostructures Based on Aromatic Peptide Amphiphiles. *Chem. Soc. Rev.* **2014**, *43*, 8150−8177.
(19) Frederix, P. W. J. M.; Scott, G. G.; Abul-Haija, Y. M.; Kalafatovic, D.; Pappas, C. G.; Javid, N.; Hunt, N. T.; Ulijn, R. V.; Tuttle, T. Exploring the Sequence Space for (Tri-)Peptide Self-Assembly to Design and Discover New Hydrogels. *Nat. Chem.* **2015**, *7*, 30−37.
(20) Smith, A. M.; Williams, R. J.; Tang, C.; Coppo, P.; Collins, R. F.; Turner, M. L.; Saiani, A.; Ulijn, R. V. Fmoc-Diphenylalanine Self Assembles to a Hydrogel via a Novel Architecture Based on Π−π Interlocked β-Sheets. *Adv. Mater.* **2008**, *20*, 37−41.
(21) Tao, K.; Levin, A.; Adler-Abramovich, L.; Gazit, E. Fmoc-Modified Amino Acids and Short Peptides: Simple Bio-Inspired Building Blocks for the Fabrication of Functional Materials. *Chem. Soc. Rev.* **2016**, *45*, 3935−3953.
(22) Yang, Z.; Gu, H.; Fu, D.; Gao, P.; Lam, J. K.; Xu, B. Enzymatic Formation of Supramolecular Hydrogels. *Adv. Mater.* **2004**, *16*, 1440−1444.
(23) Adams, D. J. Dipeptide and Tripeptide Conjugates as Low-Molecular-Weight Hydrogelators. *Macromol. Biosci.* **2011**, *11*, 160−173.
(24) Draper, E. R.; Morris, K. L.; Little, M. A.; Raeburn, J.; Colquhoun, C.; Cross, E. R.; McDonald, T. O.; Serpell, L. C.; Adams, D. J. Hydrogels Formed from Fmoc Amino Acids. *CrystEngComm* **2015**, *17*, 8047−8057.
(25) Amdursky, N.; Molotskii, M.; Aronov, D.; Adler-Abramovich, L.; Gazit, E.; Rosenman, G. Blue Luminescence Based on Quantum Confinement at Peptide Nanotubes. *Nano Lett.* **2009**, *9*, 3111−3115.
(26) Fan, Z.; Sun, L.; Huang, Y.; Wang, Y.; Zhang, M. Bioinspired Fluorescent Dipeptide Nanoparticles for Targeted Cancer Cell Imaging and Real-Time Monitoring of Drug Release. *Nat. Nanotechnol.* **2016**, *11*, 388−394.
(27) Zelzer, M.; Scurr, D. J.; Alexander, M. R.; Ulijn, R. V. Development and Validation of a Fluorescence Method to Follow the Build-up of Short Peptide Sequences on Solid 2D Surfaces. *ACS Appl. Mater. Interfaces* **2012**, *4*, 53−58.
(28) Reches, M.; Gazit, E. Casting Metal Nanowires within Discrete Self-Assembled Peptide Nanotubes. *Science* **2003**, *300*, 625−627.
(29) Singh, P.; Brar, S. K.; Bajaj, M.; Narang, N.; Mithu, V. S.; Katare, O. P.; Wangoo, N.; Sharma, R. K. Self-Assembly of Aromatic α-Amino Acids into Amyloid Inspired Nano/micro Scaled Architects. *Mater. Sci. Eng., C* **2017**, *72*, 590−600.
(30) Babar, D. G.; Sarkar, S. Self-Assembled Nanotubes from Single Fluorescent Amino Acid. *Appl. Nanosci.* **2017**, *7*, 101−107.
(31) Guerin, S.; Stapleton, A.; Chovan, D.; Mouras, R.; Gleeson, M.; McKeown, C.; Noor, M. R.; Silien, C.; Rhen, F. M. F.; Kholkin, A. L.; Liu, N.; Soulimane, T.; Tofail, S. A. M.; Thompson, D. Control of Piezoelectricity in Amino Acids by Supramolecular Packing. *Nat. Mater.* **2017**, *17*, 180−186.
(32) Kremer, J. R.; Mastronarde, D. N.; McIntosh, J. R. Computer Visualization of Three-Dimensional Image Data Using IMOD. *J. Struct. Biol.* **1996**, *116*, 71−76.
(33) Liang, C.; Ni, R.; Smith, J. E.; Childers, W. S.; Mehta, A. K.; Lynn, D. G. Kinetic Intermediates in Amyloid Assembly. *J. Am. Chem. Soc.* **2014**, *136*, 15146−15149.
(34) Reynolds, N. P.; Adamcik, J.; Berryman, J. T.; Handschin, S.; Zanjani, A. A. H.; Li, W.; Liu, K.; Zhang, A.; Mezzenga, R. Competition between Crystal and Fibril Formation in Molecular Mutations of Amyloidogenic Peptides. *Nat. Commun.* **2017**, *8*, 1338.
(35) Görbitz, C. H. The Structure of Nanotubes Formed by Diphenylalanine, the Core Recognition Motif of Alzheimer's Beta-Amyloid Polypeptide. *Chem. Commun. (Cambridge, U. K.)* **2006**, 2332−2334.
(36) Fu, Q.; Sun, W. Mie Theory for Light Scattering by a Spherical Particle in an Absorbing Medium. *Appl. Opt.* **2001**, *40*, 1354.
(37) Chen, T.-T.; Chang, I.-C.; Tsai, M.-C.; Chang, Y.-C.; Yang, M.-H.; Chen, P.-C.; Chiu, H.-T.; Lee, C.-Y. Size-Controlled Wurtzite Zinc Oxide Spheres with the Characteristics of Visible Absorption and Mie Scattering. *CrystEngComm* **2014**, *16*, 3341−3347.
(38) Yuan, W.; Zhou, N.; Shi, L.; Zhang, K. Q. Structural Coloration of Colloidal Fiber by Photonic Band Gap and Resonant Mie Scattering. *ACS Appl. Mater. Interfaces* **2015**, *7*, 14064−14071.
(39) Hsiao, Y.-C.; Lee, W. Electrically Induced Red, Green, and Blue Scattering in Chiral-Nematic Thin Films. *Opt. Lett.* **2015**, *40*, 1201.

DOI: 10.1021/acsami.8b04912
ACS Appl. Mater. Interfaces 2018, 10, 20783−20789